ChemComm

Accepted Manuscript

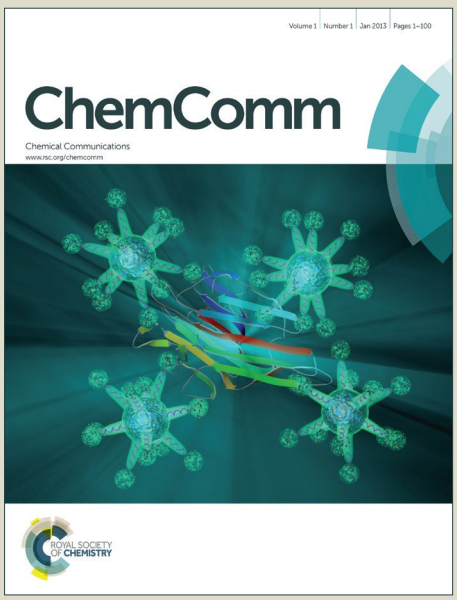

ROYAL SOCIETY OF CHEMISTRY

www.rsc.org/chemcomm

ChemComm

COMMUNICATION

Label-free ultrasensitive detection of telomerase activity *via* multiple telomeric hemin/G-quadruplexes triggered polyaniline deposition and DNA tetrahedron-structure regulated signal

Received 00th January 2015,
Accepted 00th January 2015

DOI: 10.1039/x0xx00000x

www.rsc.org/chemcomm

Yuanjian Liu,[a] Min Wei,[b] Xu Liu,[a] Wei Wei,[a]* Hongyu Zhao,[c] Yuanjian Zhang[a] and Songqin Liu[a]*

Label-free detection of telomerase activity was constructed by using telomeric hemin/G-quadruplexes triggered polyaniline deposition, not only on themselves but also on DNA tetrahedron-structure (DTS). DTS size has great impact on telomerase accessibility, reactivity and detection sensitivity. The method has been used to evaluate the bladder cancer development.

Telomerase, a ribonucleoprotein reverse transcriptase, catalyzes the addition of TTAGGG repeats to telomeric DNA to protect telomeres from erosion during cell division.[1] Telomerase activity is highly associated with the cellular immortality and carcinogenesis. In normal cells, telomerase activity is highly depressed, which leads to cell senescence and death; however, over 85% of known cancer cells overexpress the up-regulation or reactivation of telomerase activity, which makes cancer cells divide indefinitely.[2–4] Therefore, the sensitive detection of telomerase activity and its inhibition is important for diagnosis, treatment, and prognosis.[5]

Since the discovery of telomerase in 1985 by Greider and Blackburn, various strategies have been developed to determine the activity of telomerase, including polymerase chain reaction (PCR)-based telomeric repeat amplification protocol (TRAP),[4] surface plasmon resonance (SPR),[6] chemiluminescence,[7] colorimetry,[8–10] fluorescence,[11–15] nanotechnology-based methods,[16] and electrochemistry.[17–21] Among these strategies, electrochemistry has been the most extensively used research method due to its advantage of being cheap and sensitive. For example, Zhu and co-workers reported an electrochemical sensor based on spherical nucleic acids gold nanoparticles triggered mimic hybridization chain reaction.[17] Other electrochemical methods using porphyrin-graphene or luminol-gold bifunctional nanocomposites as well as hexaammineruthenium (III) chloride ($[Ru(NH_3)_6]^{3+}$, RuHex) as signal response were also developed for sensitive detection of telomerase activity.[18–20]

DNA tetrahedron-structure (DTS), which has mechanical rigidity and structural stability, has been proven to be excellent candidates to immobilize biomolecules. More recent researches have demonstrated that DNA tetrahedron-based sensor greatly increased target accessibility and reactivity.[22–26] Polyaniline (PANI) holds great promise in electrochemical sensor, due to its remarkable electrical, electrochemical and redox properties, as well as good environmental stability.[27] Nucleic acid backbones that have numerous negative charges are good templates for PANI deposition under mild conditions.[28,29] HRP mimicking DNAzyme have been substituted for HRP to catalyze the PANI deposition due to its advantages of low cost, easy synthesis and high stability.[28–31]

Inspired by the high ability of DTS to precisely control the assembly of biomolecules, its multiple nucleic acid backbones for PANI deposition and high catalysis of telomeric hemin/G-quadruplexes induced by telomerase itself, an ultrasensitive and label-free sensor for telomerase activity detection was proposed (Scheme 1). The telomerase substrate (TS) primer was designed on the top of the DTS that was constructed by four DNA strands (Table S1†), which was immobilized on the gold electrode surface *via* gold-sulfur affinity. The nanospacing between DTS-primers was precisely controlled by different size of DTS including DTS(7), DTS(13), DTS(17), DTS(26), and DTS(37), each side length of them contained 7, 13, 17, 26, and 37 base pairs, respectively. Under the action of telomerase, $(TTAGGG)_x$ were extended on the primer and then folded into multiple telomeric hemin/G-quadruplexes in the presence of hemin and potassium ions. Highest telomerase elongation efficiency and the most amount of hemin/G-quadruplexes were obtained in the presence of DTS(37), where the spacing between primers (~ 15.6 nm) was closest to the size of telomerase (~ 13 nm).[32–34] These multiple HRP-mimcking DNAzyme had high catalytic

[a] Jiangsu Province Hi-Tech Key Laboratory for Bio-medical Research, School of Chemistry and Chemical Engineering, Southeast University, Nanjing, 211189, China. E-mail: wei_wei98@163.com
[b] College of Food Science and Technology, Henan University of Technology, Zhengzhou, 450001, China
[c] Central Laboratory, The Second Affiliated Hospital of Southeast University, Nanjing, 210003, China

† Electronic Supplementary Information (ESI) available. See DOI: 10.1039/x0xx00000x

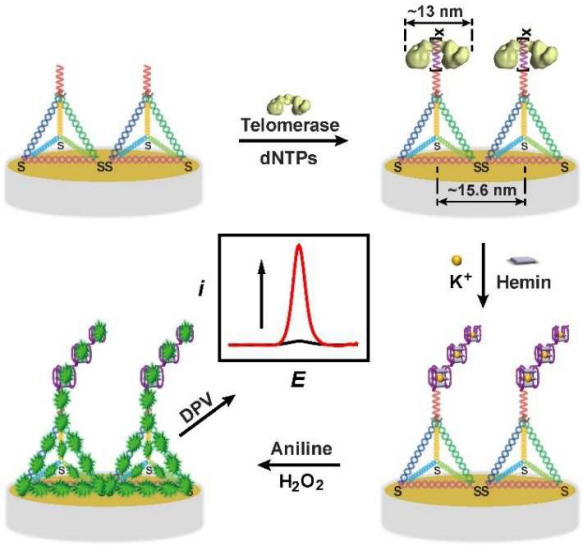

Scheme 1 Schematic illustration of label-free ultrasensitive detection of telomerase activity *via* multiple telomeric hemin/G-quadruplexes triggered PANI deposition and DTS signal regulation.

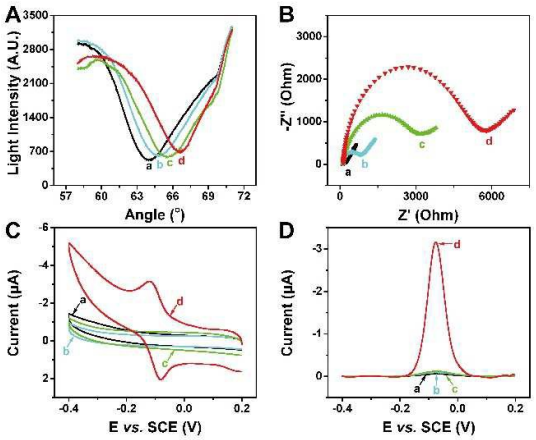

Fig. 1 (A) SPR of bare chip (a), DTS(37)-primer modified chip (b), hemin/G-quadruplex/DTS(37)-primer modified chip (c), and PANI deposition on chip (d). (B) EIS, (C) CV, and (D) DPV of bare gold electrode (a), DTS(37)-primer/gold electrode (b), telomeric repeats/DTS(37)-primer/gold electrode (c), and PANI deposition on gold electrode (d). 1 000 HeLa cells were used.

activity to initiate the PANI deposition, not only on the DTS but also on themselves. As a result, the detection sensitivity was improved to as ~ 20 times as that in the presence of single-strand DNA anchored telomerase substrate primer (ss-TS).

The assembly of the DTS-primer, formation of hemin/G-quadruplex/DTS(37)-primer and deposition of PANI were illustrated by surface plasmon resonance (SPR), electrochemical impedance spectroscopy (EIS), cyclic voltammetry (CV) and differential pulse voltammetry (DPV). The increase of the resonance angle was due to the increased mass coated to the metal surface when multiple coupling process happened. (Fig. 1A). Electron-transfer resistance (R_{et}) values also increased stepwise because the negative charges of DNA prevent repelling electrons from approaching the electrode surface (Fig. 1B). A large increased R_{et} was observed after the polymerization of PANI because large amount of PANI further inhibited the interfacial electron transfer. No CV peak was observed without the deposition of PANI (a, b, c in Fig. 1C), while a pair of new redox peaks at -0.120 V and -0.080 V appeared due to the redox of PANI (Fig. 1C, d). Differential pulse voltammetry (DPV) results were in well agreement with CV (Fig. 1D).

The effect of different sizes of DTS on telomerase accessibility, reactivity and detection sensitivity were investigated by using DTS(7), DTS(13), DTS(17), DTS(26), and DTS(37), respectively. The surface densities of the immobilized DTS-primer (number/cm^2) were quantified by chronocoulometry (CC) with a cationic redox marker of RuHex (Fig. S1A†, the calculation were showed in EIS†).[35] The surface density of the DTS-primer decreased from 9.3×10^{12}/cm^2 to 5.2×10^{11}/cm^2 with the increasing DTS size (Fig. S1B†). The distances between the primers were then calculated as about 3.7, 6.2, 7.5, 11.3, and 15.6 nm for DTS(7), DTS(13), DTS(17), DTS(26), and DTS(37), respectively, which was slightly larger than the theoretical values of 2.8, 5.1, 6.7, 10.2, and 14.5 nm (Inset in Fig. S1†). The nanospacing between the DTS(37)-primers was closest to the dimensions of telomerase (~ 13 nm), while the nanospacing between ss-TS was calculated about 1.6 nm. CC method was also used to calculate the repeat number of extension (x in $(TTAGGG)_x$) based on detection the change after the elongation.[20] (see EIS†) As shown in Fig. 2A, the charge increased obviously after the elongation. The numbers of repeats were calculated to be about 3, 5, 8, 11, 18, and 27 from ss-TS to DTS(37)-primer, respectively, which indicated that telomerase had the highest elongation efficiency in the presence of DTS(37) by minimizing the steric effect and the entanglement (Fig. 2B).

The catalysis kinetics were also strongly dependent on the distance between primers (Fig. 2C). A relatively slow catalysis process (about 100 mins) was observed when ss-TS was used, while nearly saturated signals were obtained within 40 mins when DTS(37) was used. The reaction kinetic constants (k') were obtained by supposing a pseudo-first order reaction happened. It was founded that the reaction rate was increased monotonically with the increasing DTS size (inset in Fig. 2C) and reached 0.075 min^{-1} for DTS(37).

The corresponding DPV results were showed in Fig. 2D. The currents increased with the increasing size of DTS. About -3.17 μA was obtained by using DTS(37)-primer when 1 000 HeLa cells were detected, which was hugely higher than -0.73 μA that obtained by using ss-TS. The surface morphology of formative PANI on the gold electrode surface was characterized by using scanning electron microscopy (SEM) (Fig. 2E). When ss-TS and small size of DTS were used, the polymerized PANI were deposited intermittently on the gold electrode surface. The amount of PANI increased accordance with the above obtained

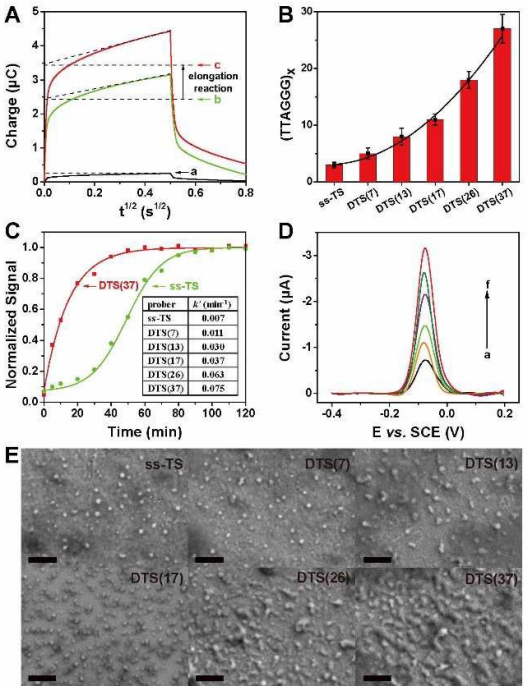

Fig. 2 (A) Chronocoulometry for the DTS(37) immobilized electrode in the absence of RuHex (a), before (b) and after elongation reaction (c) in the presence of RuHex. (B) The correlation of the number (x) of elongation in (TTAGGG)x with different size of DTS. (C) Catalysis kinetics were dependent on the DTS size. Inset: The pseudo-first-order reaction rates were shown. (D) DPV signals at different size of DTS. From a to f: ss-TS, DTS(7), DTS(13), DTS(17), DTS(26), and DTS(37). (E) SEM images of PANI deposition on gold substrate with different size of DTS. The scale bar indicates 500 nm. 1 000 HeLa cells were used.

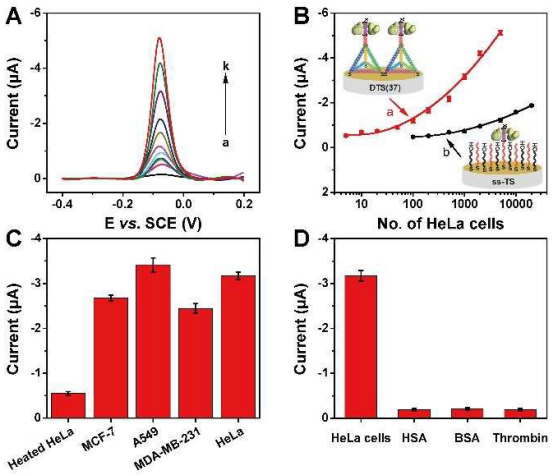

Fig. 3 (A) DPV corresponding to the different numbers of HeLa cell using DTS(37). From a to k: 0, 5, 10, 20, 50, 100, 200, 500, 1 000, 2 000, and 5 000 cells. (B) The linear plot of DPV current versus the logarithm of HeLa cell numbers ranging from 5 cells to 5 000 cells using DTS(37) (a) and 1 000 cells to 20 000 cells using ss-TS (b). (C) Telomerase activity detection in various cell lines. (D) Selectivity of the sensor for the telomerase assay. 1 000 cells were used for each cell line.

elongation efficiency, catalysis kinetics and DPV results. So, DTS(37) were selected to improve the detection sensitivity.

Fig. 3A displayed the DPV signal corresponding to different contents of HeLa cells in the presence of DTS(37). The DPV intensity increased monotonically with the logarithm number of HeLa cells (Fig. 3B, a). The dynamic range was from 5 to 5 000 HeLa cells with a detection limit of 1 HeLa cell (10 μL sample was used). As a contrast, the biosensor with ss-TS exhibited a detection limit of 20 HeLa cells (Fig. 3B, b). These results were comparable to that obtained from previously reported signal amplification methods such as exonuclease-assisted target recycling amplification (5 cells)[36] and mimic-hybridization chain reaction enzyme-free dual signal amplification (2 cells).[17] It was obviously superior to most of the methods such as the gold nanoparticle-based ECL assay (60 cells),[19] the DNAzyme-based fluorescence assay (200 cells),[37] and the quantum dot-based optical method (270 cells).[38]

Four cancer cell lines were tested. All cancer cell lines have high DPV current, while the heat-treated HeLa cells sample showed a very weak signal (Fig. 3C). It was found that telomerase activity in the HeLa and A549 cells was higher than that in MCF-7 and MDA-MB-231 cells, which were consistent with the previously reported results.[39] Selectivity and reliability of the proposed method were studied by using 3 000 HeLa cells and 100 μg of human serum albumin (HSA), bovine serum albumin (BSA), and thrombin as controls. As shown in Fig. 3D, high DPV signals were detected for HeLa cells, while very weak DPV signals were observed for HSA, BSA and thrombin, suggesting that this method had high selectivity.

Bladder cancer is the most common cancer among urogenital tumor in China and more than half of patients experienced recurrences within 5 years after initial diagnosis. With the high incidence and recurrence rate, an effective early detection and surveillance method for bladder cancer

Table 1 Comparison of the Results by Clinical Diagnosis and This Method

No.	Patient ID	Clinical outcome	DPV intensity
1	—	Normal	0.151
2	1003729557	inflammation	0.167
3	1005769946	inflammation	0.154
4	1007144483	inflammation	0.159
5	1007471636	bladder cancer II	1.349
6	1007136600	bladder cancer I	0.826
7	1004473251	bladder cancer II	1.746
8	1007137644	bladder cancer I	1.383
9	1007138928	bladder cancer II	0.909
10	1006162570	bladder cancer I	0.720
11	1007470409	bladder cancer I	1.133
12	6290036887	bladder cancer III	2.141

recurrence is urgently needed.[40] In order to demonstrate the applicability and reliability of the proposed method in clinical application, 12 bladder cancer's urine samples provided by Nanjing General Hospital of Nanjing Military Command were detected. The obtained results were showed in Table 1. A threshold of -0.267 μA, calculated from the mean DPV intensities of the PANI of 100 blank samples plus 3 times the standard deviation, was proposed to evaluate the development of the bladder cancer. According to this threshold value, negative results were obtained for normal or inflammation patients, while positive results were obtained for all bladder cancers, which were in consistent well with the clinical diagnosis results. Therefore, this electrochemical method has great potential to be developed as a noninvasive and ultrasensitive method for clinical diagnosis and evaluation of cancer development.

In summary, a novel biosensing strategy for determination of telomerase activity was developed *via* multiple telomeric hemin/G-quadruplexes induced PNAI deposition combining with DTS signal regulation. Highest telomerase elongation efficiency were obtained by using DTS(37)-primer, where the spacing between primers (~ 15.6 nm) was very close to the dimension of telomerase (~ 13 nm). The sensitivity of the sensor was greatly improved by high catalysis of multiple telomeric hemin/G-quadruplexes that elongated by telomerase themselves. Both multiple hemin/G-quadruplexes and DTS contained plenty of nucleic acid backbones that provided requisite environment for PANI deposition, which also contributed to the high sensitivity. This label-free method could detect telomerase activity in urine samples from normal, inflammation or bladder cancer patients, which is sensitive, reliable, simple, and cheap.

The project was supported by National Natural Science Foundation of China (Grant Nos. 21205014, 21475020, 21175021, 21375014).

Notes and references

1 S. B. Cohen, M. E. Graham, G. O. Lovrecz, N. Bache, P. J. Robinson and R. R. Reddel, *Science*, 2007, **315**, 1850–1853.
2 J. W. Shay and W. E. Wright, *Carcinogenesis*, 2005, **26**, 867–874.
3 F. Rodier and J. J. Campisi, *Cell Biol.*, 2011, **192**, 547–556.
4 N. W. Kim, M. A. Piatyszek, K. R. Prowse, C. B. Harley, M. D. West, P. L. Ho, G. M. Coviello, W. E. Wright, S. L. Weinrich and J. W. Shay, *Science*, 1994, **266**, 2011–2015.
5 S. C. P. Williams, *Nat. Med.*, 2013, **19**, 6.
6 C. Maesawa, T. Inaba, H. Sato, S. Iijima, K. Ishida, M. Terashima, R. Sato, M. Suzuki, A. Yashima, S. Ogasawara, H. Oikawa, N. Sato, K. Saito and T. Masuda, *Nucleic Acids Res.*, 2003, **31**, e4.
7 L. J. Wang, Y. Zhang and C. Y. Zhang, *Anal. Chem.*, 2013, **85**, 11509–11517.
8 R. De La Rica and M. M. Stevens, *Nat. Nanotechnol.*, 2012, **7**, 821–824.
9 J. S. Wang, L. Wu, J. S. Ren and X. G. Qu, *Small*, 2012, **8**, 259–264.
10 R. X. Duan, B. Y. Wang, T. C. Zhang, Z. Y. Zhang, S. F. Xu, Z. F. Chen, X. D. Lou and F. Xia, *Anal. Chem.*, 2014, **86**, 9781–9785.
11 L. L. Tian and Y. Weizmann, *J. Am. Chem. Soc.*, 2013, **135**, 1661–1664.
12 R. C. Qian, L. Ding, L. W. Yan, M. F. Lin and H. X. Ju, *J. Am. Chem. Soc.*, 2014, **136**, 8205–8208.
13 Z. X. Zhang, E. Sharon, R. Freeman, X. Q. Liu and I. Willner, *Anal. Chem.*, 2012, **84**, 4789–4797.
14 X. D. Lou, Y. Zhuang, X. L. Zuo, Y. M. Jia, Y. N. Hong, X. H. Min, Z. Y. Zhang, X. M. Xu, N. N. Liu, F. Xia and B. Z. Tang, *Anal. Chem.*, 2015, **87**, 6822–6827.
15 R. C. Qian, L. Ding, L. W. Yan, M. F. Lin and H. X. Ju, *Anal. Chem.*, 2014, **86**, 8642–8648.
16 G. F. Zheng, W. L. Daniel and C. A. Mirkin, *J. Am. Chem. Soc.*, 2008, **130**, 9644–9645.
17 W. J. Wang, J. J. Li, K. Rui, P. P. Gai, J. R. Zhang and J. J. Zhu, *Anal. Chem.*, 2015, **87**, 3019–3026.
18 L. Wu, J. S. Wang, L. Y. Feng, J. S. Ren, W. L. Wei and X. G. Qu, *Adv. Mater.*, 2012, **24**, 2447–2452.
19 H. R. Zhang, Y. Z. Wang, M. S. Wu, Q. M. Feng, H. W. Shi, H. Y. Chen and J. J. Xu, *Chem. Commun.*, 2014, **50**, 12575–12577.
20 S. Sato and S. Takenaka, *Anal. Chem.*, 2012, **84**, 1772–1775.
21 W. Q. Yang, X. Zhu, Q. D. Liu, Z. Y. Lin, B. Qiu and G. N. Chen, *Chem. Commun.*, 2011, **47**, 3129–3131.
22 Y. L. Wen, H. Pei, Y. Wan, Y. Su, Q. Huang, S. P. Song and C. H. Fan, *Anal. Chem.*, 2011, **83**, 7418–7423.
23 Z. L. Ge, M. H. Lin, P. Wang, H. Pei, J. Yan, J. Y. Sho, Q. Huang, D. N. He, C. H. Fan and X. L. Zuo, *Anal. Chem.*, 2014, **86**, 2124–2130.
24 M. H. Lin, Y. L. Wen, L. Y. Li, H. Pei, G. Liu, H. Y. Song, X. L. Zuo, C. H. Fan and Q. Huang, *Anal. Chem.*, 2014, **86**, 2285–2288.
25 G. B. Zhou, M. H. Lin, P. Song, X. Q. Chen, J. Chao, L. H. Wang, Q. Huang, W. Huang, C. H. Fan and X. L. Zuo, *Anal. Chem.*, 2014, **86**, 7843–7848.
26 X. Q. Chen, G. B. Zhou, P. Song, J. J. Wang, J. M. Gao, J. X. Lu, C. H. Fan and X. L. Zuo, *Anal. Chem.*, 2014, **86**, 7337–7342.
27 S. H. Chen, Y. J. Li and Y. L. Li, *Polym. Chem.*, 2013, **4**, 5162–5180.
28 Z. G. Wang, P. F. Zhan and B. Q. Ding, *ACS Nano*, 2013, **7**, 1591–1598.
29 Z. G. Wang, Q. Liu and B. Q. Ding, *Chem. Mater.*, 2014, **26**, 3364–3367.
30 M. Luo, X. Chen, G. H. Zhou, X. Xiang, L. Chen, X. H. Ji and Z. K. He, *Chem. Commun.*, 2012, **48**, 1126–1128.
31 T. Hou, X. J. Liu, X. Z. Wang, A. W. Jiang, S. F. Liu and F. Li, *Sens. Actuators, B: Chem.*, 2014, **190**, 384–388.
32 A. Sauerwald, S. Sandin, G. Cristofari, S. H. W. Scheres, J. Lingner and D. Rhodes, *Nat. Struct. Mol. Biol.*, 2013, **20**, 454–461.
33 E. J. Miracco, J. S. Jiang, D. D. Cash and J. Feigon, *Curr. Opin. Struct. Biol.*, 2014, **24**, 115–124.
34 S. Sandin and D. Rhodes, *Curr. Opin. Struct. Biol.*, 2014, **25**, 104–110.
35 J. Zhang, S. P. Song, L. H. Wang, D. Pan and C. H. Fan, *Nat. Protoc.*, 2007, **2**, 2888–2895.
36 H. B. Wang, S. Wu, X. Chu and R. Q. Yu, *Chem. Commun.*, 2012, **48**, 5916–5918.
37 T. Tian, S. Peng, H. Xiao, X. E. Zhang, S. Guo, S. R. Wang, X. Zhou, S. M. Liu and X. Zhou, *Chem. Commun.*, 2013, **49**, 2652–2654.
38 E. Sharon, R. Freeman, M. Riskin, N. Gil, Y. Tzfati and I. Willner, *Anal. Chem.*, 2010, **82**, 8390–8397.
39 J. S. Wang, L. Wu, J. S. Ren and X. G. Qu, *Nanoscale*, 2014, **6**, 1661–1666.
40 R. L. Liu, Z. T. Tian, J. Wang, Z. H. Zhang, Y. Xu, *Int. Urol. Nephrol.*, 2012, **44**, 1375–1382.